Catalysis Science & Technology

ROYAL SOCIETY OF CHEMISTRY

PAPER

View Article Online
View Journal | View Issue

Cite this: *Catal. Sci. Technol.*, 2023, 13, 3859

Active and durable copper phosphate catalysts modified with metal oxides for methane oxidation with oxygen into formaldehyde†

Mana Shimakawa and Sakae Takenaka*

Received 26th April 2023,
Accepted 18th May 2023

DOI: 10.1039/d3cy00573a

rsc.li/catalysis

Copper phosphates as active catalysts for methane oxidation with O_2 into formaldehyde were deposited on silica supports or dispersed with aluminum oxides in order to enhance their catalytic performance. Deposition of copper phosphates on silica led to the formation of α-$Cu_2P_2O_7$ crystallites with small sizes, which improved the formaldehyde yield in the methane oxidation with O_2. The addition of aluminum oxides into copper phosphates resulted in the formation of $Cu_3(PO_4)_2$ and α-$Cu_2P_2O_7$. These copper phosphates diluted with aluminum oxides showed high durability for the formaldehyde formation in the methane oxidation with O_2 at 923 K. These modifications of the catalysts with silica supports or alumina additives resulted in the formation of small copper phosphates crystallites and the modification of the redox performance of copper phosphates.

1. Introduction

Methane is an abundant and inexpensive resource on earth. Therefore, it is of economic and sustainable importance to find efficient ways to utilize methane.[1,2] In a conventional chemical process, methane has been converted by steam reforming into synthesis gas which is a mixture of CO and H_2. Many chemicals such as methanol and hydrocarbons have been produced from synthesis gas.[3,4] However, the steam reforming process requires a large energy input and high temperatures. Additionally, multiple steps are inevitably needed in the chemical processes for the production of methanol and hydrocarbons utilizing the synthesis gas as a feedstock. Therefore, direct conversion of methane into valuable chemicals is required, and many researchers develop catalysts effective for the partial oxidation of methane to methanol, formaldehyde, ethylene and so on.[5–7] Methane, which has strong C–H bonds (414 kJ mol^{-1}), is a chemically inert molecule and thus requires high temperatures and high pressures for its activation. Even if oxygenates such as methanol and formaldehyde were formed in the oxidation of methane with O_2 over catalysts, these products are easily oxidized into carbon monoxide and carbon dioxide over catalysts due to severe conditions such as high temperatures and high pressures, which makes it difficult to develop effective catalysts for the partial oxidation of methane.[8,9] It was reported that metal oxides of Co, V, Mo and Fe supported on silica are effective for the partial oxidation of methane.[10–13] For example, high yields of formaldehyde with 1–2% have been observed in the methane oxidation with O_2 over VO_x/SiO_2 and MoO_x/SiO_2 catalysts at 903 K.[14] It is generally accepted that active species for partial oxidation of methane into formaldehyde are highly dispersed metal oxide clusters such as tetrahedral VO_4 on silica, while aggregated metal oxides catalyse the total oxidation of methane into CO_2. Bulk crystallized $FePO_4$ was also reported as active catalysts for the formaldehyde formation, showing a formaldehyde yield of 0.2% in methane oxidation at 673–723 K.[15] Some research groups investigated the catalytic performance of Cu oxide clusters for the partial oxidation of methane. CuO_x with low loading on the mesoporous silica SBA-15 catalysed the formaldehyde formation at 1% yield in the methane oxidation with O_2 at 898 K.[16] CuO_x stabilized in zeolites has been also attracting attention as catalysts capable of selective conversion of methane into formaldehyde and methanol at temperatures as low as 573 K.[17] The catalysts formed methanol and formaldehyde selectively at low temperatures, but treatment of the catalysts with water vapor was required for the desorption of oxygenate products from the catalysts after being in contact with fresh catalysts with methane.[18] As described earlier, many catalysts have been developed for the direct conversion of methane into valuable chemicals by oxidation with O_2, but further improvement of catalytic performance should be required for the utilization of methane as chemical feedstock.

Faculty of Science and Engineering, Doshisha University, Tatara-Miyakodani 1-3, Kyotanabe, Kyoto 610-0321, Japan. E-mail: stakenak@mail.doshisha.ac.jp

† Electronic supplementary information (ESI) available. See DOI: https://doi.org/10.1039/d3cy00573a

We have also focused on copper oxides as catalytically active components for the partial oxidation of methane with O_2. We reported that crystallized $Cu_3Mo_2O_9$ in copper–molybdenum complex oxides and α-$Cu_2P_2O_7$ in copper phosphate catalysts are particularly effective for formaldehyde formation in the oxidation of methane with O_2.[19,20] However, these catalysts showed low activity for the reaction, which would be due to their low surface areas. Additionally, high durability of these Cu-based crystallites for sintering should be required because methane oxidation with O_2 is performed at high temperatures and the active components for the reaction are repeatedly reduced with methane and oxidized with O_2 during the reaction. In the present study, copper phosphates were stabilized on silica supports or dispersed with aluminum oxides in order to increase their surface areas and improve their stability at high temperatures. This modification of the copper phosphates enhanced their catalytic activity and durability for the partial oxidation of methane into formaldehyde.

2. Experimental

2.1 Preparation of silica-supported $CuPO_x$ catalysts

Silica-supported $CuPO_x$ catalysts ($CuPO_x/SiO_2$) were prepared by an impregnation method. Silica powder was impregnated into an aqueous solution containing copper nitrate, ammonium dihydrogen phosphate and malic acid and dried up at 353 K. The samples thus obtained were calcined in air at 973 K. Two types of silicas (JRC-SIO12 and JRC-SIO9A, specific surface area of 79 and 333 $m^2\ g^{-1}$, respectively; reference catalysts of The Catalysis Society of Japan) were used as supports for copper phosphates. $CuPO_x/SiO_2$ catalysts with different $CuPO_x$ loadings and different molar ratios of Cu to P were prepared. Bulk copper phosphates (α-$Cu_2P_2O_7$ and $Cu(PO_3)_2$) were also prepared as control samples with a similar method to the preparation of $CuPO_x/SiO_2$.

2.2 Preparation of copper phosphates modified with aluminum oxides

Copper phosphates modified with aluminum oxides (AlO_x) (AlO_x–$CuPO_x$) were prepared by a coprecipitation method. Copper nitrate, ammonium dihydrogen phosphate, and aluminum nitrate were dissolved in pure water (0.5 M), and then aqueous ammonia was added into the solution to obtain precipitates. The precipitates thus obtained were calcined at 973 K in air to obtain AlO_x–$CuPO_x$.

2.3 Oxidation of methane with O_2

Oxidation of methane with O_2 was performed in a flow reactor with a fixed catalyst bed. Catalyst powder (0.050 g) diluted with quartz sands was packed in the catalyst bed of a quartz reactor. The catalyst was treated at 973 K in O_2 diluted with He prior to the oxidation of methane. For the oxidation of methane, a mixed gas composed of methane, O_2 and He ($CH_4 : O_2 : He = 1 : 1 : 5$) was in contact with the fresh catalysts at 823 K. During the reaction, the temperatures of the catalyst bed were changed to 873, 923 and 973 K. The effluent gases from the catalyst bed were passed through the traps cooled at 200 K to condense oxygenate products such as formaldehyde and methanol. The gases through the cold traps were analyzed by gas chromatographs with a TCD and FID. O_2, CO and CO_2 in the effluent gases were analyzed using columns packed with activated carbon and molecular sieve 5A. CH_4, C_2H_4 and C_2H_6 were separated using a column packed with Porapak Q. The concentration of formaldehyde contained in the cold traps was evaluated with UV-vis spectroscopy. The products in the cold traps were added to mixed aqueous solutions of ammonium acetate, acetic acid and acetylacetone at 333 K, to form 3,5-diacetyl-1,4-dihydrolutidine.[21] The concentration of formaldehyde was evaluated from the absorption at 413 nm due to 3,5-diacetyl-1,4-dihydrolutidine formed from formaldehyde in the UV-vis spectra for the solutions.

2.4 Characterization of the catalysts

X-ray diffraction (XRD) patterns of the catalysts were collected at room temperature (Rigaku MiniFlex 600, Cu Kα radiation, λ = 1.54 Å). The crystal phases of the catalysts were identified using the powder diffraction file (PDF) database of the International Centre for Diffraction Data (ICDD). The profiles of temperature-programmed reduction (TPR) with H_2 for the catalysts were obtained by heating the catalyst samples from room temperature up to 873 K at a heating rate of 10 K min^{-1} in the stream of H_2 diluted with Ar. Prior to the measurement of the TPR profiles, the catalyst samples were treated with O_2 at 973 K. The consumption of H_2 during the TPR experiments was monitored using a TCD.

3. Results and discussion

3.1 Catalytic performance of $CuPO_x/SiO_2$

$CuPO_x/SiO_2$ catalysts with various molar ratios of Cu/(Cu + P) were prepared, while the total loading of Cu and P was fixed to 10 wt% for the catalysts. The $CuPO_x/SiO_2$ catalysts with molar ratio of Cu/(Cu + P) = 0.25, 0.33, 0.50 and 0.60 were denoted as Cu(25)-PO_x/SiO_2, Cu(33)-PO_x/SiO_2, Cu(50)-PO_x/SiO_2, and Cu(60)-PO_x/SiO_2, respectively. Fig. 1 shows the XRD patterns for the $CuPO_x/SiO_2$ catalysts. Only diffraction peaks assignable to α-$Cu_2P_2O_7$ were observed at around 2θ = 28 and 30 degrees in the XRD patterns for Cu(25)-PO_x/SiO_2, Cu(33)-PO_x/SiO_2 and Cu(50)-PO_x/SiO_2 catalysts (PDF No. 01-071-2177), whereas the peaks corresponding to CuO were also found in addition to those corresponding to α-$Cu_2P_2O_7$ in the XRD pattern for Cu(60)-PO_x/SiO_2. The crystallized compounds confirmed in the XRD patterns and specific surface areas evaluated by nitrogen adsorption at 77 K for the catalysts are summarized in Table 1. The formation of α-$Cu_2P_2O_7$ only was confirmed as copper phosphates in the XRD patterns for all the $CuPO_x/SiO_2$ catalysts in spite of the molar ratios of Cu/(Cu + P). In contrast, various copper phosphates such as $Cu(PO_3)_2$, α-$Cu_2P_2O_7$ and $Cu_3(PO_4)_2$ were

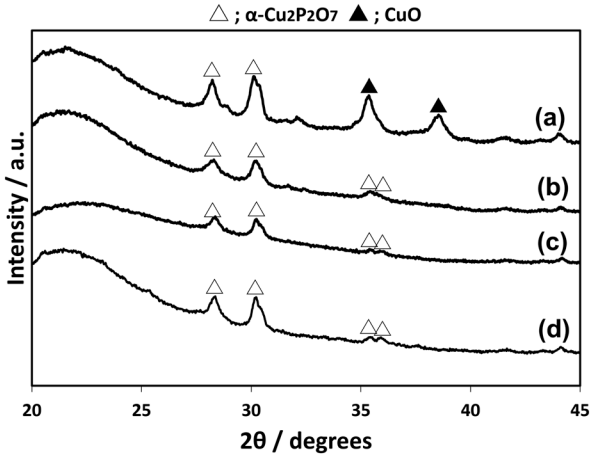

Fig. 1 XRD patterns of $CuPO_x/SiO_2$ catalysts with different molar ratios of Cu/(Cu + P). a) Cu(60)-PO_x/SiO_2, b) Cu(50)-PO_x/SiO_2, c) Cu(33)-PO_x/SiO_2, and d) Cu(25)-PO_x/SiO_2.

Table 1 Surface area and crystallized phase for $CuPO_x/SiO_2$ catalysts with different molar ratios of Cu/(Cu + P)

Catalyst	Surface area [$m^2\ g^{-1}$]	Main phase
Cu(25)-PO_x/SiO_2	120	α-$Cu_2P_2O_7$
Cu(33)-PO_x/SiO_2	55	α-$Cu_2P_2O_7$
Cu(50)-PO_x/SiO_2	55	α-$Cu_2P_2O_7$
Cu(60)-PO_x/SiO_2	64	α-$Cu_2P_2O_7$·CuO
PO_x/SiO_2	59	Amorphous
CuO_x/SiO_2	69	CuO
SiO_2	79	Amorphous
$Cu(PO_3)_2$	1	$Cu(PO_3)_2$
α-$Cu_2P_2O_7$	11	α-$Cu_2P_2O_7$
$Cu_3(PO_4)_2$	6	$Cu_3(PO_4)_2$

formed according to the molar ratio in the bulk copper phosphates without silica.

Table 2 and Fig. S1† show the results of the oxidation of methane over $CuPO_x/SiO_2$ catalysts with different molar ratios of Cu/(Cu + P). Formaldehyde was selectively formed in the methane oxidation over silica and silica-supported PO_x catalysts (PO_x/SiO_2), but their catalytic activity was very low. Thus, the formaldehyde yield was also quite low (0.1%) for both the catalysts. On the other hand, silica-supported CuO_x catalysts (CuO_x/SiO_2) showed higher activity for methane oxidation than silica and PO_x/SiO_2, but the selectivity to formaldehyde was quite low, and instead, CO_2 was selectively formed. Methane conversion and selectivity to each product in the methane oxidation over $CuPO_x/SiO_2$ catalysts strongly depended on the molar ratio of Cu/(Cu + P). Generally, the catalytic activity became higher, and the selectivity to formaldehyde became lower as the Cu/(Cu + P) ratio in the $CuPO_x/SiO_2$ catalysts was higher. It should be noted that formaldehyde yield attained 0.9% in the methane oxidation over Cu(33)-PO_x/SiO_2 catalysts at 923 K. The formaldehyde yield for Cu(33)-PO_x/SiO_2 was higher than that for bulk α-$Cu_2P_2O_7$ catalysts without silica supports as shown in Fig. S1,† although the weight of copper phosphates packed in the catalyst bed was very low in the reaction over Cu(33)PO_x/SiO_2 compared with that over bulk α-$Cu_2P_2O_7$, since the weight of the catalyst powder packed in the reactors was the same for both the catalysts. As shown in Table 2 and Fig. S1,† α-$Cu_2P_2O_7$ is the most active catalyst for the formation of formaldehyde in the methane oxidation among all the bulk copper phosphate catalysts tested in the present study.[20] These results indicated that copper phosphates α-$Cu_2P_2O_7$ dispersed on the silica support also work as catalytically active sites for the formation of formaldehyde.

Table 2 Methane oxidation over $CuPO_x/SiO_2$ catalysts with different molar ratios of Cu/(Cu + P)

Catalyst	Temp. [K]	Conversion [%]	Selectivity [%]			HCHO yield [%]
			HCHO	CO	CO_2	
Cu(25)-PO_x/SiO_2	873	0.6	72	0	28	0.4
	923	2.0	48	2	50	1.0
Cu(33)-PO_x/SiO_2	873	0.8	53	0	47	0.4
	923	3.3	28	55	17	0.9
Cu(50)-PO_x/SiO_2	873	1.5	34	0	66	0.5
	923	3.6	23	0	78	0.8
Cu(60)-PO_x/SiO_2	873	1.4	18	0	82	0.2
	923	3.3	13	4	83	0.4
PO_x/SiO_2	873	0.0	100	0	0	0.0
	923	0.1	100	0	0	0.1
CuO_x/SiO_2	873	0.5	13	0	87	0.1
	923	1.0	11	0	89	0.1
SiO_2	873	0.04	100	0	0	0.04
	923	0.1	100	0	0	0.1
$Cu(PO_3)_2$	873	0.03	100	0	0	0.03
	923	0.06	100	0	0	0.06
α-$Cu_2P_2O_7$	873	1.2	38	55	7	0.5
	923	4.1	19	68	13	0.8
$Cu_3(PO_4)_2$	873	1.8	4	1	95	0.06
	923	1.8	11	6	83	0.2

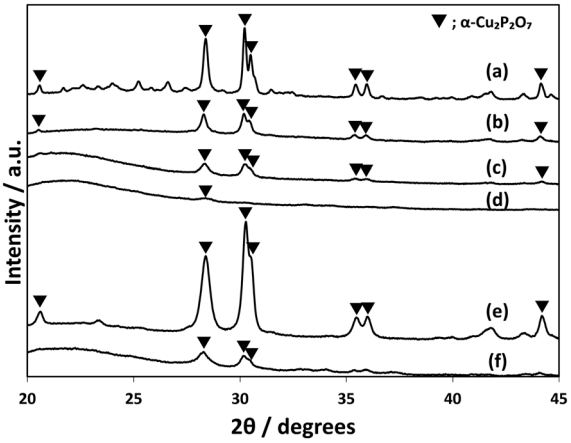

Fig. 2 XRD patterns of $CuPO_x/SiO_2$ with different loadings. a) $CuPO_x$(80 wt%)/l-SiO_2, b) $CuPO_x$(60 wt%)/l-SiO_2, c) $CuPO_x$(10 wt%)/l-SiO_2, d) $CuPO_x$(6 wt%)/l-SiO_2, e) $CuPO_x$(60 wt%)/h-SiO_2, and f) $CuPO_x$(20 wt%)/h-SiO_2.

The catalytic performance of $CuPO_x/SiO_2$ with different loadings for methane oxidation was evaluated. Two types of silicas (specific surface area of 79 and 333 $m^2\ g^{-1}$) were used as supports for copper phosphates. $CuPO_x$ of 6, 10, 60, and 80 wt% was loaded on silica with a low surface area, and these catalysts were denoted as $CuPO_x$(*Y* wt%)/l-SiO_2 (*Y* stands for the $CuPO_x$ loading). On the other hand, $CuPO_x$ of 20 and 60 wt% were supported on silica with high surface area, and the catalysts were denoted as $CuPO_x$(*Y* wt%)/h-SiO_2. For all $CuPO_x/SiO_2$ with different loadings, the molar ratio of Cu/(Cu + P) was fixed to 0.33. Fig. 2 shows the XRD patterns of $CuPO_x/SiO_2$ with different loading. In the XRD patterns for all the $CuPO_x/SiO_2$ catalysts in Fig. 2, only the diffraction peaks corresponding to α-$Cu_2P_2O_7$ were observed, and these peaks became sharper with the $CuPO_x$ loading. Table 3 shows the specific surface area of each catalyst and an average crystallite size of α-$Cu_2P_2O_7$ evaluated from the width at half-maxima of their diffraction lines. The results clearly showed that the average size of the α-$Cu_2P_2O_7$ crystallite became larger with the $CuPO_x$ loading in the catalysts.

Table 4 and Fig. S2† show the results of the methane oxidation over $CuPO_x/SiO_2$ catalysts with different loadings. Methane conversion gradually increased, and the selectivity to formaldehyde decreased as the $CuPO_x$ loading became higher. As described earlier, α-$Cu_2P_2O_7$ with a larger crystallite size was supported on silica with the loading in the $CuPO_x/SiO_2$ catalysts. Thus, the difference in the catalytic performance of $CuPO_x/SiO_2$ with different loadings would result from the crystallite size of α-$Cu_2P_2O_7$. It is interesting that the formaldehyde yield in the reaction over $CuPO_x/SiO_2$ catalysts with low loadings, for example, $CuPO_x$(10 wt%)/l-SiO_2 and $CuPO_x$(20 wt%)/h-SiO_2 was higher than that in the reaction over the bulk α-$Cu_2P_2O_7$ catalysts although the amount of $CuPO_x$ packed in the catalyst bed for the former catalyst was only 10–20% of that for the latter one, as clarified from Table 4 and Fig. S2.† Thus, we conclude that deposition of small α-$Cu_2P_2O_7$ crystallites on silica supports is effective for the design of $CuPO_x$ catalysts active for methane oxidation into formaldehyde.

Fig. 3 shows the change of the selectivity to formaldehyde (panel a), CO (panel b) and CO_2 (panel c) and the formaldehyde yield (panel d) as a function of the *W*/*F* value (*W*, weight of catalysts in the catalyst bed; *F*, flow rate of the reactant gas) in the methane oxidation over $CuPO_x$ (20 and 60 wt%)/h-SiO_2 and bulk α-$Cu_2P_2O_7$ catalysts at 923 K. As the *W*/*F* value became lower, selectivity to formaldehyde increased, and instead, the selectivity to CO_2 decreased in the methane oxidation over all the catalysts shown in Fig. 3. In particular, formaldehyde was selectively formed in the reaction over $CuPO_x$(60 wt%)/h-SiO_2 catalysts at a low *W*/*F* value, which means short contact time of the reactant gases with the catalysts. These results suggest that formaldehyde is the primary product in methane oxidation over the $CuPO_x/SiO_2$ catalysts. Successive oxidation of oxygenate products during the methane oxidation should be inhibited by the deposition of small α-$Cu_2P_2O_7$ crystallites onto the silica supports.

Temperature-programed reduction (TPR) with H_2 for $CuPO_x/SiO_2$ catalysts was performed to clarify the difference in the catalytic performance between $CuPO_x$ stabilized on silica supports and bulk copper phosphates. Fig. 4 shows the TPR profiles for various $CuPO_x/SiO_2$ catalysts and bulk copper phosphates ($Cu(PO_3)_2$ and α-$Cu_2P_2O_7$). In the TPR profiles for the $CuPO_x/SiO_2$ catalysts, a peak due to the reduction of copper phosphates with hydrogen was observed in the temperature range from 700 to 950 K, and its position was shifted toward higher temperatures with the $CuPO_x$ loadings. These peaks should be assignable to the reduction of copper oxides surrounded with phosphates.[22,23] As described earlier,

Table 3 Surface area and an average crystallite size for $CuPO_x/SiO_2$ with different $CuPO_x$ loadings

Catalyst	Main phase	Crystallite size [Å]	Surface area [$m^2\ g^{-1}$]
$CuPO_x$(6 wt%)/l-SiO_2	α-$Cu_2P_2O_7$	97	66
$CuPO_x$(10 wt%)/l-SiO_2	α-$Cu_2P_2O_7$	113	55
$CuPO_x$(60 wt%)/l-SiO_2	α-$Cu_2P_2O_7$	227	16
$CuPO_x$(80 wt%)/l-SiO_2	α-$Cu_2P_2O_7$	340	2
$CuPO_x$(20 wt%)/h-SiO_2	α-$Cu_2P_2O_7$	113	48
$CuPO_x$(60 wt%)/h-SiO_2	α-$Cu_2P_2O_7$	227	25
α-$Cu_2P_2O_7$	α-$Cu_2P_2O_7$	205	11
$Cu(PO_3)_2$	$Cu(PO_3)_2$	466	1

Table 4 Methane oxidation over $CuPO_x/SiO_2$ catalysts with different loadings

Catalyst	Temp. [K]	Conversion [%]	Selectivity [%]			HCHO yield [%]
			HCHO	CO	CO_2	
$CuPO_x$(6 wt%)/l-SiO_2	873	1.5	33	11	56	0.5
	923	4.5	19	63	18	0.8
$CuPO_x$(10 wt%)/l-SiO_2	873	0.8	53	0	47	0.4
	923	3.3	28	55	17	0.9
$CuPO_x$(60 wt%)/l-SiO_2	873	0.1	100	0	0	0.1
	923	0.9	86	1	13	0.8
$CuPO_x$(80 wt%)/l-SiO_2	873	0.1	100	0	0	0.1
	923	0.2	59	23	19	0.2
$CuPO_x$(20 wt%)/h-SiO_2	873	1.3	40	0	60	0.5
	923	3.7	24	0	77	0.9
$CuPO_x$(60 wt%)/h-SiO_2	873	0.5	69	0	31	0.3
	923	1.7	48	6	47	0.8
α-$Cu_2P_2O_7$	873	1.2	38	55	7	0.5
	923	4.1	19	68	13	0.8
$Cu(PO_3)_2$	873	0.03	100	0	0	0.03
	923	0.06	100	0	0	0.06

α-$Cu_2P_2O_7$ crystallites were present on silica for all the $CuPO_x/SiO_2$ shown in Fig. 2, and their average crystallite size became larger with $CuPO_x$ loadings. Thus, smaller α-$Cu_2P_2O_7$ crystallites should be reduced with hydrogen at lower temperatures.[24] It should be noted that bulk α-$Cu_2P_2O_7$ is reduced with hydrogen at lower temperatures than $CuPO_x$(60 w%)/l-SiO_2 and $CuPO_x$(60 w%)/h-SiO_2, although the average crystallite size of α-$Cu_2P_2O_7$ was very similar for these catalysts. Chemical interaction between α-$Cu_2P_2O_7$ and silica supports should cause the change in the redox properties of $CuPO_x$. The formation of small α-$Cu_2P_2O_7$ crystallites and their chemical interaction with silica would lead to the selective formation of formaldehyde, as well as the inhibition of its successive oxidation into CO and CO_2 in the methane oxidation with O_2.

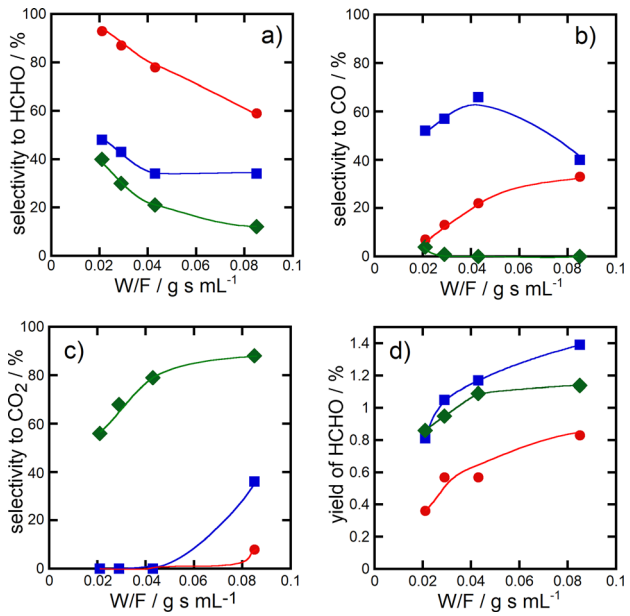

Fig. 3 Change of the selectivity to formaldehyde (panel a), CO (panel b) and CO_2 (panel c) and HCHO yield (panel d) as a function of *W*/*F* value in the methane oxidation over $CuPO_x$ catalysts at 923 K. ■ $CuPO_x$(20 wt%)/h-SiO_2, ● $CuPO_x$(60 wt%)/h-SiO_2, and ◆ α-$Cu_2P_2O_7$.

3.2 Catalytic performance of AlO_x-$CuPO_x$

$CuPO_x$ catalysts were modified with different metal oxides (MgO_x, AlO_x, CrO_x, MnO_x and SrO_x) to enhance their catalytic performance. The results are shown in Table S1 (ESI†). The loading of metal oxides added in $CuPO_x$ catalysts (molar ratio of Cu/(Cu + P) = 0.5) was fixed to 10 mol% for all the catalysts shown in Table S1.† The addition of AlO_x enhanced the catalytic activity of $CuPO_x$ for the methane oxidation, while the selectivity to formaldehyde was not changed significantly by the addition of AlO_x. In contrast, the modification with MgO_x, CrO_x, MnO_x and SrO_x decreased the catalytic activity of $CuPO_x$ for methane oxidation. Thus, the formaldehyde

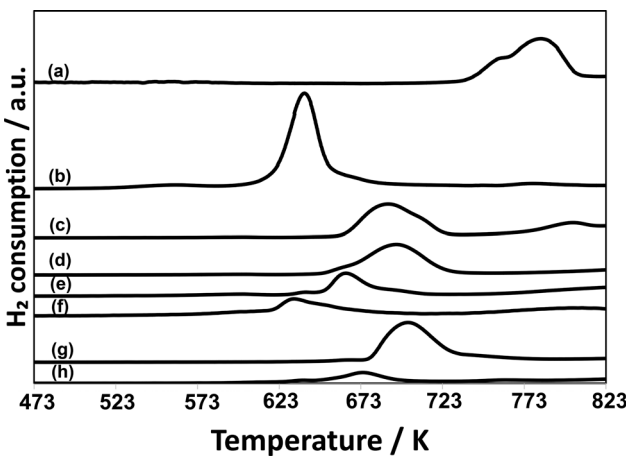

Fig. 4 TPR profiles for $CuPO_x/SiO_2$ catalysts with different loadings. a) $Cu(PO_3)_2$, b) α-$Cu_2P_2O_7$, c) $CuPO_x$(80 wt%)/l-SiO_2, d) $CuPO_x$(60 wt%)/l-SiO_2, e) $CuPO_x$(10 wt%)/l-SiO_2, f) $CuPO_x$(6 wt%)/l-SiO_2, g) $CuPO_x$(60 wt%)/h-SiO_2, and h) $CuPO_x$(20 wt%)/h-SiO_2.

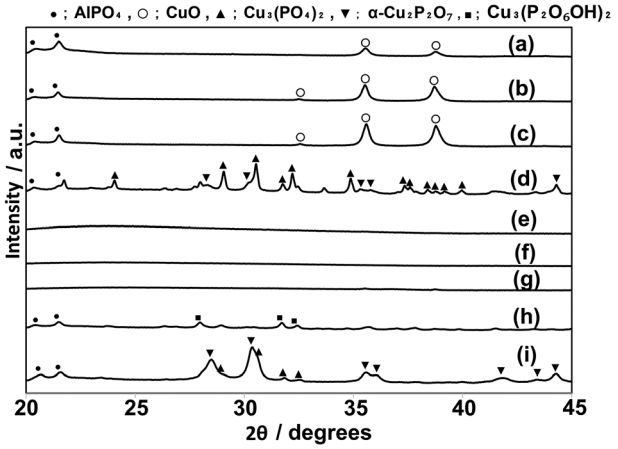

Fig. 5 XRD patterns of AlO_x–$CuPO_x$ catalysts. a) Cu(10)-P(45)-Al(45), b) Cu(50)-P(25)-Al(25), c) Cu(80)-P(10)-Al(10), d) Cu(45)-P(45)-Al(10), e) Cu(25)-P(25)-Al(50), f) Cu(10)-P(10)-Al(80), g) Cu(45)-P(10)-Al(45), h) Cu(25)-P(50)-Al(25), and i) Cu(10)-P(80)-Al(10).

Table 5 Specific surface areas of AlO_x–$CuPO_x$

Catalyst	Surface area [m^2 g^{-1}]	Main phase
Cu(10)-P(45)-Al(45)	80	CuO
Cu(50)-P(25)-Al(25)	26	CuO
Cu(80)-P(10)-Al(10)	8	CuO
Cu(45)-P(45)-Al(10)	15	$Cu_3(PO_4)_2$
Cu(25)-P(25)-Al(50)	81	Amorphous
Cu(10)-P(10)-Al(80)	286	Amorphous
Cu(45)-P(10)-Al(45)	105	Amorphous
Cu(25)-P(50)-Al(25)	39	$Cu_3(P_2O_6OH)_2$
Cu(10)-P(80)-Al(10)	11	α-$Cu_2P_2O_7$
α-$Cu_2P_2O_7$	11	α-$Cu_2P_2O_7$
$Cu_3(PO_4)_2$	3	$Cu_3(PO_4)_2$
CuO	4	CuO

yields in the reaction over $CuPO_x$ catalysts with these additives were lower than that over the catalysts without additives. It was reported that the addition of AlO_x into metal oxides suppresses their sintering during the catalytic reactions at high temperatures.[25,26] Thus, we evaluated the catalytic performance of $CuPO_x$ catalysts modified with aluminum oxides (AlO_x) in detail.

AlO_x of different amounts was added into copper phosphates to increase their specific surface areas. The molar ratios of Cu, Al and P in AlO_x–$CuPO_x$ catalysts are denoted as Cu(x)-Al(y)-P(z) (x, y and z are mol% of Cu, Al, and P, respectively). Fig. 5 shows XRD patterns of different AlO_x–$CuPO_x$ catalysts. Based on the results of these XRD patterns, AlO_x–$CuPO_x$ catalysts were classified into three types. In the XRD patterns for Cu(25)-P(25)-Al(50), Cu(10)-P(10)-Al(80), and Cu(45)-P(10)-Al(45), any diffraction lines were not observed, indicating that structures of these catalysts were amorphous. In the XRD patterns for Cu(10)-P(45)-Al(45), Cu(50)-P(25)-Al(25), and Cu(80)-P(10)-Al(10), the diffraction peaks corresponding to any crystallized copper phosphates were not observed, but those corresponding to $AlPO_4$ and CuO were observed. In contrast, Cu(45)-P(45)-Al(10), Cu(25)-P(50)-Al(25), and Cu(10)-P(80)-Al(10) catalysts were composed of crystallized copper phosphates. Cu(45)-P(45)-Al(10) catalysts contained crystallized $Cu_3(PO_4)_2$ in addition to small amounts of α-$Cu_2P_2O_7$ and $AlPO_4$. The main component in Cu(25)-P(50)-Al(25) catalysts was $Cu_3(P_2O_6OH)_2$. On the other hand, crystallized α-$Cu_2P_2O_7$ was mainly present in addition to a small amount of $Cu_3(PO_4)_2$ and $AlPO_4$ in Cu(10)-P(80)-Al(10) catalysts. As clarified in Table 5, the specific surface areas for AlO_x–$CuPO_x$ with amorphous structures were relatively higher than those for the other catalysts. Although the surface areas of AlO_x–$CuPO_x$ catalysts with crystallized compounds were low, their surface areas were slightly larger than those for bulk copper phosphates without AlO_x.

Table 6 and Fig. S3† show the results of the methane oxidation over AlO_x–$CuPO_x$ catalysts containing crystallized copper phosphates in addition to the results on the bulk α-$Cu_2P_2O_7$, $Cu_3(PO_4)_2$ and CuO catalysts. Cu(25)-P(50)-Al(25) catalysts showed the highest activity for methane oxidation among all the catalysts in Table 6, but methane was completely oxidized with O_2 into CO_2 over the catalysts. It is likely that $Cu_3(P_2O_6OH)_2$ in the catalysts catalyzes the total oxidation of methane into CO_2. In contrast, the selectivity to formaldehyde in the reaction over the other AlO_x–$CuPO_x$

Table 6 Methane oxidation over AlO_x–$CuPO_x$ catalysts

Catalyst	Temp. [K]	Conversion [%]	Selectivity [%]			HCHO yield [%]
			HCHO	CO	CO_2	
Cu(45)-P(45)-Al(10)	873	2.4	30	14	56	0.7
	923	6.6	16	19	65	1.0
Cu(25)-P(50)-Al(25)	873	9.9	0	0	100	0.2
	923	21.8	0	0	100	0.2
Cu(10)-P(80)-Al(10)	873	1.2	43	5	52	0.5
	923	3.5	22	9	69	0.8
α-$Cu_2P_2O_7$	873	1.2	38	55	7	0.5
	923	4.1	19	68	13	0.8
CuO	873	2.1	1	0	99	0.0
	923	2.7	2	0	98	0.1
$Cu_3(PO_4)_2$	873	0.3	25	6	75	0.1
	923	1.0	20	10	75	0.2

catalysts was significantly higher than that over Cu(25)-P(50)-Al(25) catalysts. The catalytic performance of Cu(10)-P(80)-Al(10) for the reaction was very similar to that of bulk α-$Cu_2P_2O_7$ catalysts, which showed the highest yield of formaldehyde in the methane oxidation among all the bulk copper phosphate catalysts tested in the present study. High yield of formaldehyde should be obtained in the reaction over Cu(10)-P(80)-Al(10) catalysts since the catalysts were composed of α-$Cu_2P_2O_7$ active for the partial oxidation of methane into formaldehyde. It is interesting that the Cu(45)-P(45)-Al(10) also showed higher activity for the reaction compared to the bulk copper phosphate catalysts, and the selectivity to formaldehyde was also relatively high. Thus, a formaldehyde yield of 1.0% was obtained in the reaction over the catalysts at 923 K. As described earlier, the Cu(45)-P(45)-Al(10) catalysts are composed of $Cu_3(PO_4)_2$. The methane conversion was very low in the methane oxidation over bulk $Cu_3(PO_4)_2$ catalysts without AlO_x additives at 873 and 923 K. This would be due to the low surface area of bulk $Cu_3(PO_4)_2$. AlO_x additives would prevent the sintering of $Cu_3(PO_4)_2$ crystallites during the preparation of the catalysts and the methane oxidation at high temperatures.

Table S2 (ESI†) shows the results of the oxidation of methane over other AlO_x–$CuPO_x$ catalysts in addition to the catalysts shown in Table 6. These catalysts are composed of amorphous compounds or mixtures of CuO and $AlPO_4$. As clarified from the results in Table S2,† these catalysts showed high activity for methane oxidation, but selectivity to formaldehyde and its yield were quite low. Thus, we conclude that α-$Cu_2P_2O_7$ and $Cu_3(PO_4)_2$ work as catalytically active components for methane oxidation into formaldehyde.

Fig. 6 shows change of the selectivity to formaldehyde, CO and CO_2 (panel a) and the formaldehyde yield (panel b) as a function of *W*/*F* value in the methane oxidation over Cu(45)-P(45)-Al(10) catalysts at 923 K. The selectivity to formaldehyde became lower and instead that to CO_2 became higher with W/F values, suggesting that formaldehyde was the primary product in the methane oxidation over the catalysts. Formaldehyde was successively oxidized with O_2 into CO_2 over the catalysts.

The addition of AlO_x into $CuPO_x$ also improved the durability of the catalysts during the methane oxidation.

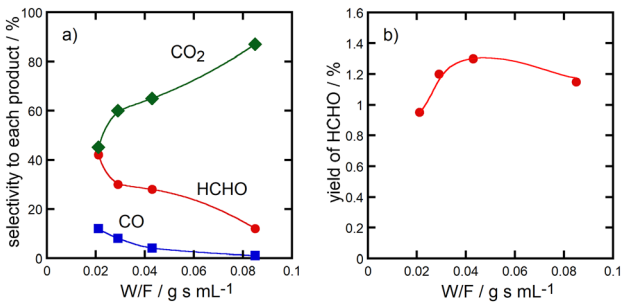

Fig. 6 Change of the selectivity to formaldehyde, CO and CO_2 (panel a) and the HCHO yield (panel b) as a function of *W*/*F* value in the methane oxidation over Cu(45)-Al(45)-P(10) catalysts at 923 K.

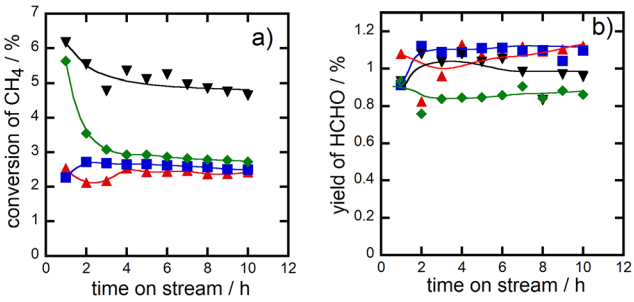

Fig. 7 Change of methane conversion (panel a) and formaldehyde yield (panel b) as a function of time on stream in the methane oxidation over the copper phosphate catalysts at 923 K. ▲ $CuPO_x$(10 wt%)/l-SiO_2, ■ $CuPO_x$(20 wt%)/h-SiO_2, ▼ Cu(45)-P(45)-Al(10), and ◆ α-$Cu_2P_2O_7$.

Fig. 7 showed the change of methane conversion (panel a) and formaldehyde yield (panel b) as a function of time on stream in the methane oxidation over α-$Cu_2P_2O_7$ and Cu(45)-P(45)-Al(10) catalysts at 923 K, in addition to the results of the reaction over $CuPO_x$(10 wt%)/l-SiO_2 and $CuPO_x$(20 wt%)/h-SiO_2 catalysts. Methane conversion in the reaction over bulk α-$Cu_2P_2O_7$ catalyst was rapidly decreased for 2 h after the reactants were contacted with the fresh catalyst and then it was kept to 3% for 10 h. Both $CuPO_x/SiO_2$ catalysts showed high durability for the reaction although the methane conversion over these catalysts was not so high compared to those over the other catalysts. AlO_x–$CuPO_x$ (Cu(45)-P(45)-Al(10)) was also deactivated slightly at the early period of the reaction, but the methane conversion over the catalysts was always higher than those over the other catalysts. Thus, formaldehyde yields in the reaction over $CuPO_x$(10 wt%)/l-SiO_2, $CuPO_x$(20 wt%)/h-SiO_2 and Cu(45)-P(45)-Al(10) are always higher than that in the reaction over bulk α-$Cu_2P_2O_7$ catalyst. The deactivation of the catalyst should result from the sintering of copper phosphates which worked as active components for the reaction. AlO_x additives in copper phosphates suppress the contact between copper phosphate crystallites during the methane oxidation at 923 K, which improves the durability of the catalysts.

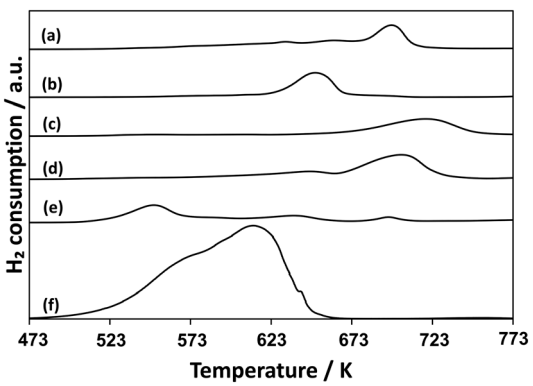

Fig. 8 TPR profiles for AlO_x–$CuPO_x$ catalysts. a) $Cu_3(PO_4)_2$, b) α-$Cu_2P_2O_7$, c) Cu(10)-P(80)-Al(10), d) Cu(45)-P(45)-Al(10), e) Cu(25)-P(50)-Al(25), and f) CuO.

Fig. 8 shows TPR profiles for AlO_x–$CuPO_x$ catalysts and the reference samples. Cu(25)-P(50)-Al(25) catalysts, which showed the highest activity for the total oxidation of methane into CO_2 among all the AlO_x–$CuPO_x$ catalysts in Table 6, were reduced with H_2 at lower temperatures. The high redox property of copper phosphates in Cu(25)-P(50)-Al(25) catalysts would lead to the high selectivity to the total oxidation in the methane oxidation with O_2. In contrast, Cu(45)-P(45)-Al(10) and Cu(10)-P(80)-Al(10) catalysts, which showed high selectivity to formaldehyde in the methane oxidation, were reduced with H_2 at higher temperatures than the bulk copper phosphates shown in Fig. 8. As described earlier, the deposition of $CuPO_x$ on silica decreased their activity for the reduction with H_2. The control of the redox property of $CuPO_x$ by the addition of AlO_x or by the deposition onto silica supports is effective for the development of active $CuPO_x$ catalysts for the partial oxidation of methane with O_2 into formaldehyde. The deposition onto silica supports or the addition of AlO_x should result in the formation of copper phosphates with smaller crystallite sizes as well as chemical interaction with silica or aluminum oxide. The interaction should prevent the total oxidation of methane into CO_2 and the sintering of copper phosphates in the catalysts during the methane oxidation at high temperatures.

Conclusion

Copper phosphates as catalysts for the methane oxidation with O_2 into formaldehyde were supported on silica or were modified with aluminum oxide (AlO_x) to improve the catalytic activity and durability. Deposition of copper phosphates on silica supports led to the formation of α-$C_2P_2O_7$ crystallites with small sizes while crystallized $Cu_3(PO_4)_2$ with a high surface area was stabilized in the copper phosphate catalysts modified with AlO_x. Copper phosphate catalysts supported on silica or modified with AlO_x formed formaldehyde with a yield of 1.1–1.4% by methane oxidation. These modifications with silica or AlO_x resulted in the control of the redox properties of copper phosphates.

Author contributions

M. Shimakawa carried out and interpreted the experimental part. S. Takenaka conceived the idea and supervised the whole project. Both authors have contributed and agreed with the final version of the manuscript.

Conflicts of interest

There are no conflicts to declare.

Acknowledgements

This work was supported by JSPS KAKENHI Grant Numbers 20H02526 and 23H01766.

Notes and references

1 A. Demirbas, *Energy Convers. Manage.*, 2010, **51**, 1547–1561.
2 M. J. G. Fait, A. Ricci, M. Holena, J. Rabeah, M.-M. Pohl, D. Linke and E. V. Kondratenko, *Catal. Sci. Technol.*, 2019, **9**, 5111–5121.
3 P. Schwach, X. Pan and X. Bao, *Chem. Rev.*, 2017, **117**, 8497–8520.
4 M. J. G. Fait, A. Ricci, M. Holena, J. Rabeah, M.-M. Pohl, D. Linke and E. V. Kondratenko, *Catal. Sci. Technol.*, 2019, **9**, 5111–5121.
5 J. T. Grant, J. M. Venegas, W. P. McDermott and I. Hermans, *Chem. Rev.*, 2018, **118**, 2769–2815.
6 E. V. Kondratenko, T. Peppel, D. Seeburg, V. A. Kondratenko, N. Kalevaru, A. Martin and S. Wohlrab, *Catal. Sci. Technol.*, 2017, **7**, 366–381.
7 Z. Guo, B. Liu, Q. Zhang, W. Deng, Y. Wang and Y. Wang, *Chem. Rev.*, 2014, **43**, 3480–3524.
8 A. Matsuda, H. Tateno, K. Kamata and M. Hara, *Catal. Sci. Technol.*, 2021, **11**, 6987–6998.
9 M. J. G. Fait, A. Ricci, M. Holena, J. Rabeah, M.-M. Pohl, D. Linke and E. V. Kondratenko, *Catal. Sci. Technol.*, 2019, **9**, 5111–5121.
10 L. D. Nguyen, S. Loridant, H. Launay, A. Pigamo, J. L. Dubois and J. M. M. Millet, *J. Catal.*, 2006, **237**, 38–48.
11 J. Ohyama, D. Abe, A. Hirayama, H. Iwai, Y. Tsuchimura, K. Sakamoto, M. Irikura, Y. Nakamura, H. Yoshida, M. Machida, S. Nishimura, T. Yamamoto and K. Takahashi, *J. Phys. Chem. C*, 2022, **126**, 1785–1792.
12 V. Foréns, C. López, H. H. López and A. Martínez, *Appl. Catal., A*, 2003, **249**, 345–354.
13 J. He, Y. Li, D. An, Q. Zhang and Y. Wang, *J. Nat. Gas Chem.*, 2009, **18**, 288–294.
14 R. G. Herman, Q. Sun, C. Shi, K. Klier, C. Wang, H. Hu, I. E. Wachs and M. M. Bhasin, *Catal. Today*, 1997, **37**, 1–14.
15 Y. Wang and K. Otsuka, *J. Catal.*, 1995, **155**, 256–267.
16 L. Yang, A. Dongli, Q. Zhang and Y. Wang, *J. Phys. Chem. C*, 2008, **112**, 13700–13708.
17 M. H. Groothaert, P. J. Smeets, B. F. Sels, P. A. Jacobs and R. A. Schoonheydt, *J. Am. Chem. Soc.*, 2005, **127**, 1394–1395.
18 J. Ohyama, A. Hirayama, Y. Tsuchimura, N. Kondou, H. Yoshida, M. Machida, S. Nishimura, K. Kato, I. Miyazato and K. Takahashi, *Catal. Sci. Technol.*, 2021, **11**, 3437–3446.
19 T. Akiyama, R. Sei and S. Takenaka, *Catal. Sci. Technol.*, 2021, **51**, 5273–5281.
20 T. Akiyama, M. Shimakawa and S. Takenaka, *Chem. Lett.*, 2022, **51**, 511–514.
21 T. Nash, *Biochem. J.*, 1953, **55**, 416–421.
22 C. Sepúlveda, L. Delgado, R. García, M. Melendrez, J. L. G. Fierro, I. T. Ghampson and N. Escalona, *Catal. Today*, 2017, **279**, 217–223.
23 H. Li, F. Wang, W. Cai, J. Zhang and X. Zhang, *Catal. Sci. Technol.*, 2015, **5**, 5174–5184.
24 S. Takenaka, T. Kaburagi, C. Yamada, K. Nomura and K. Otsuka, *J. Catal.*, 2004, **228**, 66–74.
25 S. Takenaka, M. Serizawa and K. Otsuka, *J. Catal.*, 2004, **222**, 520–531.
26 S. Takenaka, K. Nomura, N. Hanaizumi and K. Otsuka, *Appl. Catal., A*, 2005, **282**, 333–341.

